Nonlinear Phase Field Model for Electrodeposition in Electrochemical systems

Linyun Liang[1,2,a)], Long-Qing Chen[1]

[1]*Department of Materials Science and Engineering, The Pennsylvania State University,*

University Park, Pennsylvania 16802, USA

[2]*Mathematics and Computer Science Division, Argonne National Laboratory, Argonne, Illinois,*

60439, USA

Abstract: A nonlinear phase-field model has been developed for describing the electrodeposition process in electrochemical systems that are highly out of equilibrium. Main thermodynamic driving forces for the electrode-electrolyte interface (EEI) evolution are limited to local variations of overpotential and ion concentration. Application of the model to Li-ion batteries describes the electrode interface motion and morphology change caused by charge mass transfer in the electrolyte, an electrochemical reaction at the EEI and cation deposition on the electrode surface during the charging operation. The Li electrodeposition rate follows the classical Butler-Volmer kinetics with exponentially and linearly depending on local overpotential and cation concentration at the electrode surface, respectively. Simulation results show that the Li deposit forms a fiber-like shape and grows parallel to the electric field direction. The longer and thicker deposits are observed both for higher current density and larger rate constant where the surface reaction rate is expected to be high. The proposed diffuse interface model well captures the metal electrodeposition phenomena in plenty of non-equilibrium electrochemical systems.

Electrochemical deposition of metals and alloys is a versatile technique that enables the application of protective/conductive coatings on metallic or other conductive surfaces which involves the reduction of metal ions from aqueous, organic and fused-salt electrolytes. During the course of electrodeposition the surface of deposits usually becomes inhomogeneous and produces irregular shapes. Such complex self-organized patterns generated far from the equilibrium state have fascinated scientists for decades due to their remarkable effects on physical and chemical properties of the system. For example, in Li-ion batteries, the formation of Li deposits leads to a large decrease of reversible capacity and worst a short-circuiting phenomenon as deposits grow towards to the cathode.[1-5] During the electrodeposition process, it is believed that the morphology and growth of electrodeposits are mainly determined by the kinetics of the heterogeneous electrode reaction, electrode surface states, Ohmic potential drop and mass species transports in the electrochemical system. Therefore, it is critical to understand the underlying physical mechanisms of such complex non-equilibrium system and learn how to control morphologies and evolutions of those rough electrodeposits to improve the properties of materials.

Plenty of studies have been dedicated to study the morphology instability during electrodeposition processes. Experimental approaches were employed to study the formation mechanism and morphology of deposits such as transmission electron

microscopy (TEM),[6, 7] optical microscopy,[8, 9] and in situ scanning electron microscopy (SEM).[10, 11] On the other hand, various of models including mathematical models[12-17] and meso-scale models[18-24] have been developed to understand and predict the relationship between the deposit morphology and growth and the transport-reaction processes. However, generally speaking, all existing models are either difficult to handle the electrode-electrolyte interface (EEI) evolution and its morphology change or only assuming a linear reaction kinetic or not capturing the electrochemical process at the moving interface from the physical nature.

In this letter, we present a nonlinear phase-field model for understanding the metal electrodeposition behaviors when the system is highly out of equilibrium. The Li electrodeposition at the anode in Li-ion batteries during the charging operation is taking as an example. The electrochemical reaction at the EEI, ionic species diffusion, and electric potential distribution are taken into account in this model. For simplicity, we don't consider the solid electrolyte interface (SEI) properties in this work although it plays an important role in the initiation or nucleation of deposits.[25]

Two phases, metal phase (α phase) and electrolyte phase (β phase), are considered in the system. The metal phase is composed of pure Li, while the electrolyte phase includes cation (Li^+) and anion (PF_6^-) species, and electrons (e^-) are assumed to be always supplied on the electrode surface as shown in Fig. 1. The system is assumed to be isothermal. At the electrode surface Li^+ is deposited via the following chemical reaction,

$$Li^+ + e^- \leftrightarrow Li \; , \tag{1}$$
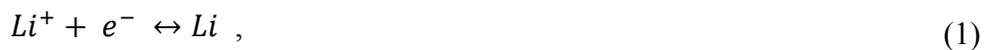
where the forward reaction only occurs when the overpotential is greater than the equilibrium potential (0 V) or fast charging process (overcharge).

Based on the nonlinear phase-field equation developed for the EEI evolution,[26] the effects of local variations of reactant and product concentrations and overpotential on the interface evolutions are incorporated in the current model. As we known that the reaction kinetic at the electrode surface following the fundamental relationship is $v = k_f C_{Li}^s - k_b C_{Li^+}^s$, where k_f and k_b are forward and backward reaction rates, $C_{Li^+}^s$ and C_{Li}^s are concentrations of Li^+ and Li at the electrode surface, respectively.[27] Therefore, the nonlinear phase-field equation can be formulated as,

$$\frac{\partial \xi(r,t)}{\partial t} = -L_\sigma \frac{\delta \Sigma}{\delta \xi} - L_\eta RT h'(\xi) \left[\frac{C_{Li}^S(r,t)}{C_{Li}^0} exp\left(\frac{\alpha \Delta G(r,t)}{RT}\right) - \frac{C_{Li}^S(r,t)}{C_{Li^+}^0} exp\left(-\frac{\beta \Delta G(r,t)}{RT}\right) \right], \qquad (2)$$

where the phase parameter $\xi(r,t)$ is used to distinguish the electrolyte and electrode phases, L_σ is interface mobility, L_η is rate constant, and Σ is the total interfacial free energy given by $\Sigma = \int_V \left[g(\xi) + \frac{1}{2}\kappa(\theta)(\nabla\xi(r,t))^2 \right] dV$, $h(\xi)$ is $\xi^3(6\xi^2 - 15\xi + 10)$ and $g(\xi)$ is $W\xi^2(\xi - 1)^2$. Anisotropy surface energy is introduced to represent the roughness of the electrode surface, which is given by $\kappa(\theta) = \kappa_0[1 + \delta\cos(\lambda\theta)]$, where δ and λ is the strength and mode of the anisotropy interface energy, κ_0 is a constant, θ is the angle between the normal vector of interface and a certain direction.[28] $C_{Li^+}^0$ and C_{Li}^0 are the Li^+ and Li bulk concentrations, respectively. The activation energy $\Delta G(r,t) = zF\eta(r,t)$ is related to the overpotential $\eta(r, t)$, where z is the valence of Li atom, α and β are transfer constants. Therefore, the rate of phase parameter change follows the classical Butler-

Volmer kinetic, in which the reaction rate is exponentially and linearly depending on the overpotential and concentration, respectively. This equation can be considered as the diffuse-interface type of Butler-Volmer equation that allows the interface evolution driven by the gradient of cation concentration and overpotential.

The electrolyte solution is assumed to be relative dilute. The diffusion of Li^+ and PF_6^- concentrations can be described as,

$$\frac{\partial C_c(r,t)}{\partial t} = \nabla \cdot \left(D_c \nabla C_c(r,t) + \mu_c C_c(r,t) \nabla \phi(r,t) \right), \tag{3}$$

$$\frac{\partial C_a(r,t)}{\partial t} = \nabla \cdot \left(D_a \nabla C_a(r,t) - \mu_a C_a(r,t) \nabla \phi(r,t) \right), \tag{4}$$

where C_c and C_a, D_c and D_a, and μ_c and μ_a are cation and anion concentrations, diffusivities and mobilities, respectively, $\phi(r,t)$ is an electric potential. A charge neutrality condition is imposed, i.e., $z_a C_a \approx z_c C_c \approx C_{Li^+}$. To simplify the model, we eliminate the potential-dependent term to lead to a simple ambipolar diffusion equation, $\partial C_{Li^+}(r,t)/\partial t = \nabla \cdot \left(D^L \nabla C_{Li^+}(r,t) \right)$ with $D^L = \left(D_a \mu_a + D_c \mu_c \right)/\left(\mu_a + \mu_c \right).$[29] Then we rewrite the Li^+ diffusion equation as,

$$\frac{\partial C_{Li^+}(r,t)}{\partial t} = \nabla \cdot \left(D(\xi) \nabla C_{Li^+}(r,t) \right) - \dot{R}_{Li^+}(r,t), \tag{5}$$

where the diffusivity is $D(\xi) = D^S h(\xi) + D^L \left(1 - h(\xi) \right)$, D^S is the Li^+ diffusivity in the electrode which is almost zero. $\dot{R}_{Li^+}$ describes the accumulation/elimination of Li^+ due to the chemical reaction at EEI. It is related to the Li^+ concentration and reaction rate, where

the reaction rate is related to the phase change rate $\partial \xi(r,t)/\partial t$ in Eq. (2). Thus, the source term in Eq. (5) can be expressed as $\dot{R}_{Li^+}(r,t) = \varepsilon^{-1} C_{Li^+}^S(r,t)\partial \xi(r,t)/\partial t$, where ε is the thickness of EEI.

The flow of current is continuous everywhere. The current conservation is assumed in the system, which can be described as,

$$\nabla \cdot \left[\sigma(\xi)\nabla(\varphi(r,t)) - i_{reaction}(r,t)\right] = 0 \, ,\tag{6}$$

where the conductivity is $\sigma(\xi) = \sigma^S h(\xi) + \sigma^L(1 - h(\xi))$, σ^S and σ^L are the electrode and electrolyte conductivities, respectively, $i_{reaction}$ is a source term to describe the reaction current generated by the chemical reaction at EEI. Similarly, this source term is related to the reaction rate $\partial \xi(r,t)/\partial t$ in Eq. (2) having a form, $i_{reaction} = i_0/RTM_\xi \, \partial \xi(r,t)/\partial t$, where i_0 is the exchange current density, $i_0 = Fk(C_t - C_{Li})^\alpha (C_{Li})^\beta (C_{Li^+})^\alpha$, where k is rate constant, C_t is the maximum concentration in electrode. It should be noted that the above proposed equation can fully describe the continuous current flow in the electrochemical system due to the cations motion in the electrolyte, electrons motion in the electrode and electrochemical reaction at the electrolyte/electrode interface.

Above three equations [Eqs. (2, 5, 6)] are correlated by the chemical reaction term. Boundary conditions are given as follows. In Eq. (2), a constant current i_n is applied at the electrolyte side, $D^L F/(1 - t^0) \partial C_{Li^+}/\partial x\big|_{x=Lx} = i_n$. In Eq. (6), constant electric potentials are assumed at both the electrode and electrolyte sides. And the rest boundaries are zero-flux conditions. The Tridiagonal Matrix Algorithm (TDMA) is employed to solve equations in two dimensions. Parameters used are $C_{Li^+}^0 = 0.5$ M, $D^L = 2.6 \times 10^{-6} cm^2 s^{-1}$,[30]

$D^S = 2.6 \times 10^{-6} cm^2 s^{-1}$, $\sigma_\alpha = 1.1 \times 10^7 Sm^{-1}$, $\sigma_{electrolyte} = 1.0 \times 10^{-3} Sm^{-1}$ [31]

$T = 298\ K$, $\gamma = 1.716\ Jm^{-1}$ [16] $\Omega = 1.31 \times 10^{-5} m^{-3}$, $\lambda = 4.0$, $\delta = 0.05$, $\alpha = \beta = 0.5$,

$W = 5.0$, $L_\sigma = 0.5$. The dimensionless evolution time is $t^* = D_0 t / L^2$. The dimensionless

rate constant is defined as $r = i_0 / RTL_\sigma$. Other used parameters include the time step

$t^* = 0.005$, the grid size $\Delta x = \Delta y = 0.001$.

We firstly start with a planar interface to illustrate the evolutions of phase parameter, Li^+ concentration and electric potential by solving three coupled Eqs. (2, 5, 6). Simulation results along the x direction at two different time steps are shown in Fig. 2. Three variables develop diffuse interfaces across the EEI. Li^+ concentration in the vicinity of electrode is expected to be zero and gradually increases apart from the electrode, which is consistent with the experimental observations.[32] The total electric potential drop in the system includes three parts as shown in Fig.3, i. e., the potential drop in the electrolyte due to the ion conduction, the potential drop across the interface due to the electrochemical reaction and the Omic potential drop in the electrode where it is almost flat because of the high conductivity of Li. In a diffuse interface description, the overpotential is taken as a field which is obviously different from the sharp-interface model that is usually taken as a single value by the potential difference between the electrode and electrolyte as illustrated in Fig.2. The overpotential is automatically taken as the driving force based on Eq. (2). The growth of Li deposit starts when the overpotential reaches zero. As shown in Fig. 2 the EEI moves along with time caused by depositing Li^+ on the electrode surface. The Li^+ concentration increases with time due to the amount of consuming of Li^+ at EEI is less than the amount of coming from the electrolyte side. We also observe that the maximum value of overpotential slightly

increases along with time,[33] which corresponds to the reaction rate increase because of the increase of Li^+ concentration.

The calculated velocities of deposits as a function of time under different applied current densities and rate constants are shown in Fig. 3. The velocity change is almost linear at the initial stage because of the small overpotential and low Li^+ concentration, but it is accelerated with respect to time as the deposit approaches the cathode side.[16, 34] Consistent with the mathematical model, the deposition velocity has a nonlinear relationship with the time.[16] At a constant reaction rate, the increase of current density leads to the increase of deposit velocity, and also the earlier nucleation and formation of deposits. Similarly, a larger deposit velocity is obtained under a faster reaction rate charged at a constant current density. As expected, for both large reaction rate and current density, the rate of Li deposition is high and leads to a rapid depletion of Li^+ in the system and form a thicker deposited film.

The current density at the tip of deposit related to the electrodeposition velocity can be estimated by $i_{tip} = v_{tip}zF/V_m$,[35] where V_m is the molar volume of Li atom. Therefore, the current density at the tip of deposit has the same trend with the velocity. With the time increase, the current density produces a nonlinear relationship with the overpotential, which is considered to be satisfied the Butler-Volmer kinetics. The validation is performed by comparing phase-field results with the Butler-Volmer equation using the same concentration, which are given in Fig. 3.

During the charging operation, the growth of surface is directly related to the local variation of current density. The current density in turn can be related to the Li^+

concentration and electric potential by reaction kinetics in which surface tension also appears. This results in a concentration gradient in the neighborhood of the electrode and/or the deposit. Figure 4 shows the evolution of a single deposit, as well as the Li^+ concentration and electric potential. It is well known that the SEI film has non-uniform ion conductivities. The transport and accumulation of Li^+ in the SEI layer leads to the nucleation and growth of Li deposits that may break the SEI film. Thus, the deposition points are the points where the higher Li^+ conductivity of SEI film.[36] We start with a seed particle to represent a single broken point of the SEI film. Along with time evolution, as shown in Fig. 4, the deposit develops a fiber-like morphology whithout branching, which agrees with the experiemental observations.[9, 37-39] The fiber grows parallel to the direction of the electric field. Typically there are concentration and potential gradients that distabilize the EEI. The evolution of Li^+ concentration and electric potential clearly shows the local variations of current density and overpotential. The potential drop at the interface is strongly inhomogeneous. Based on the Butler-Volmer equation, this can be attributed to the inhomogeneous current densities that caused by the anisotropic interface energy and Li^+ concentration gradient. The tip of deposit has the larger concentration gradient and overpotential that produces the larger deposition rate and forces it to grow faster. Therefore, the front of Li deposit grows much faster than the behind once its initiallisation. Surface tension acts to stabilize the electrode surface but it is effective only for a very small wavelength perturbation.

Figure 5 shows the effects of different current densities and rate constants on morphologies of formed deposits at a certain time step. The EEI is unstable for all cases. The local inhomogeneities of deposits are expected to induce local variations of current

density, hence of the concentration gradient. Because of the electrochemical reaction, the deposit grows with Li ions deposition. Simultaneously, part of Li ions can be deposited onto electrode surface to form the continuous dense lithium layer. However, the growth of dense layer is relatively slow compared with the growth of deposit due to the inhomogeneity of current densities. Very large current density and rate constant gives large deposit growth rate. Therefore, longer and thicker deposits are obtained at a larger current density than the smaller one as shown in Fig. 5 (a).[40, 41] The deposits with kinks are also obtained at a larger current density caused by their faster growth and the interactions between nearby deposits. It is noteworthy that the growth of deposit has a very strong directional tendency. The existence of large concentration gradient in the front of the growing deposit accelerates its growth.[42] Our calculation results also indicate that the faster of Li^+ diffusion the denser of deposits are observed. Similarly, a larger rate constant leads to a faster electrodeposition and longer deposit as shown in Fig.5 (b). When the cell is discharging, the deposit is dissolved and mostly isolated from the base to form "dead lithium". As a result, the cell life becomes shorter due to the electrochemical inactive of "dead lithium" and consumption of active material. If the deposit morphology is formed as a dense layer, the Li-ion battery can have a longer life cycle and better thermal stability. Therefore, the optimization of the charging condition and electrolyte solution can effectively reduce the fiber-like deposit nucleation and growth to improve the cell's life.

In summary, a nonlinear phase-field model has been developed to capture the electrode-electrolyte interface motion and its morphology evolution during the electrochemical deposition involving highly non-equilibrium processes. Without

considering the solid-electrolyte interface layer effect, the model can simulate and predict the Li deposit formation and growth in Li-ion batteries during the charging operation. The electrodeposition rate implicitly follows the Butler-Volmer kinetic. To further consider the deposit formation on the graphite anode, the diffusion of Li inside the graphite needs to be incorporated in the current model. Beyond the Li electrodeposition in Li-ion batteries, our methodology can be used to simulate other non-equilibrium systems in which the electrochemical reaction and charge mass transfer play important roles, if involved interfaces are diffuse and time-dependent.

ACKNOWLEDGMENTS

[a])Author to whom correspondence should be addressed. Electronic mail: lyliang39@gmail.com.

1.   R. Selim and P. Bro, Journal of the Electrochemical Society **121** (11), 1457-1459 (1974).
2.   K. M. Abraham, J. Power Sources **14** (1-3), 179-191 (1985).
3.   D. Aurbach, E. Zinigrad, H. Teller and P. Dan, Journal of the Electrochemical Society **147** (4), 1274-1279 (2000).
4.   J. B. Goodenough and Y. Kim, Chem. Mat. **22** (3), 587-603 (2010).
5.   J. M. Tarascon and M. Armand, Nature **414** (6861), 359-367 (2001).
6.   I. Epelboin, M. Froment, M. Garreau, J. Thevenin and D. Warin, J. Electrochem. Soc. **127**, 2100 (1980).
7.   D. Grier, E. Benjacob, R. Clarke and L. M. Sander, Physical Review Letters **56** (12), 1264-1267 (1986).
8.   M. Arakawa, S. Tobishima, Y. Nemoto, M. Ichimura and J. Yamaki, J. Power Sources **43**, 27 (1993).
9.   K. Nishikawa, T. Mori, T. Nishida, Y. Fukunaka, M. Rosso and T. Homma, Journal of the Electrochemical Society **157** (11), A1212-A1217 (2010).
10.   M. Dolle, L. Sannier, B. Beaudoin, M. Trentin and J. M. Tarascon, Solid-State Lett. **5**, A286 (2002).
11.   M. Rosso, C. Brissot, A. Teyssot, M. Dolle, L. Sannier, J. M. Tarascon, R. Bouchetc and S. Lascaud, Electrochimica Acta **51** (25), 5334-5340 (2006).
12.   M. Ramasubramanian, B. N. Popov, R. E. White and K. S. Chen, Journal of the Electrochemical Society **146** (1), 111-116 (1999).
13.   J. N. Chazalviel, Physical Review A **42** (12), 7355-7367 (1990).

14.   W. Q. Lu, C. M. Lopez, N. Liu, J. T. Vaughey, A. Jansen and D. W. Dees, Journal of the Electrochemical Society **159** (5), A566-A570 (2012).
15.   R. D. Perkins, A. V. Randall, X. C. Zhang and G. L. Plett, Journal of Power Sources **209**, 318-325 (2012).
16.   C. Monroe and J. Newman, Journal of the Electrochemical Society **150** (10), A1377-A1384 (2003).
17.   M. Tang, P. Albertus and J. Newman, J. Electrochem. Soc. **156**, A390 (2009).
18.   M.-O. Bernard, M. Plapp and J.-F. Gouyet, Phys. Rev. E **68**, 011604 (2003).
19.   Y. Shibuta, Y. Okajima and T. Suzuki, Sci. Tech. Advan. Mater. **8**, 511 (2007).
20.   W. Pongsaksawad, A. C. P. IV and D. Dussault, J. Electrochem. Soc. **154**, F122 (2007).
21.   J. E. Guyer, W. J. Boettinger and J. A. Warren, Phys. Rev. E **69**, 021603 (2004).
22.   J. E. Guyer, W. J. Boettinger and J. A. Warren, Phys. Rev. E **69**, 021604 (2004).
23.   D. Josell, D. Wheeler, W. H. Huber and T. P. Moffat, Phys. Rev. Lett. **87**, 016102 (2001).
24.   Y. Shibuta, T. Sato, T. Suzuki, H. Ohta and M. Kurata, J. Nucl. Mater. **436** (1-3), 61-67 (2013).
25.   E. Peled, Journal of the Electrochemical Society **126** (12), 2047-2051 (1979).
26.   L. Y. Liang, Y. Qi, F. Xue, S. Bhattacharya, S. J. Harris and L. Q. Chen, Physical Review E **86** (5) (2012).
27.   J. Newman and K. E. Thomas-Alyea, *Electrochemistry System* (John Wiley & Sons, Inc., Hoboken, New Jersey, 2004).
28.   W. J. Boettinger, J. A.Warren, C. Beckermann and A. Karma, Annu. Rev. Mater. Res. **32**, 163 (2002).
29.   C. Brissot, M. Rosso, J. N. Chazalviel and S. Lascaud, Journal of the Electrochemical Society **146** (12), 4393-4400 (1999).
30.   K. Smith and C. Y. Wang, J. Power Sources **161** (1), 628-639 (2006).
31.   V. Zadin, H. Kasemagi, A. Aabloo and D. Brandell, J. Power Sources **195** (18), 6218-6224 (2010).
32.   C. Brissot, M. Rosso, J. N. Chazalviel and S. Lascaud, J. Power Sources **94** (2), 212-218 (2001).
33.   V. R. Subramanian, V. Boovaragavan, V. Ramadesigan and M. Arabandi, Journal of the Electrochemical Society **156** (4), A260-A271 (2009).
34.   P. Arora, M. Doyle and R. E. White, Journal of the Electrochemical Society **146** (10), 3543-3553 (1999).
35.   O. Crowther and A. C. West, Journal of the Electrochemical Society **155** (11), A806-A811 (2008).
36.   K. Nishikawa, T. Mori, T. Nishida, Y. Fukunaka and M. Rosso, J. Electroanal. Chem. **661** (1), 84-89 (2011).
37.   J. Yamaki, S. Tobishima, K. Hayashi, K. Saito, Y. Nemoto and M. Arakawa, J. Power Sources **74** (2), 219-227 (1998).
38.   K. Kanamura, S. Shiraishi and Z. Takehara, Journal of the Electrochemical Society **143** (7), 2187-2197 (1996).
39.   H. Ghassemi, M. Au, N. Chen, P. A. Heiden and R. S. Yassar, Applied Physics Letters **99** (12) (2011).
40.   M. Dolle, L. Sannier, B. Beaudoin, M. Trentin and J. M. Tarascon, Electrochemical and Solid State Letters **5** (12), A286-A289 (2002).
41.   K. Nishikawa, H. Naito, M. Kawase and T. Nishida, in *Rechargeable Lithium and Lithium Ion Batteries*, edited by M. K. Sunkara, M. C. Smart, R. V. Bugga, K. M. Abraham and R. Brodd (Electrochemical Soc Inc, Pennington, 2012), Vol. 41, pp. 3-10.
42.   K. Nishikawa, Y. Fukunaka, T. Sakka, Y. H. Ogata and J. R. Selman, Journal of the Electrochemical Society **154** (10), A943-A948 (2007).